UPSCALING SAPFLOW MEASUREMENTS TO FOOTPRINT TRANSPIRATION ESTIMATIONS IN THE JORNADA EXPERIMENTAL RANGE, NEW MEXICO, USA

HABIBUR RAHMAN HOWLIDER

Master's Program in Environmental Science

APPROVED:

Hernan A. Moreno, Ph.D., Chair

Hugo A. Gutierrez, Ph.D.

Marguerite E. Mauritz, Ph.D.

Stephen L. Crites, Jr., Ph.D.
Dean of the Graduate School

to my

WIFE and Two Beautiful Boys "IZHAAN" and "IBTIHAJ"

with love

UPSCALING SAPFLOW MEASUREMENTS TO FOOTPRINT TRANSPIRATION ESTIMATIONS IN THE JORNADA EXPERIMENTAL RANGE, NEW MEXICO, USA

by

HABIBUR RAHMAN HOWLIDER

THESIS

Presented to the Faculty of the Graduate School of

The University of Texas at El Paso

in Partial Fulfillment

of the Requirements

for the Degree of

MASTER OF SCIENCE

Department of Earth, Environmental and Resource Sciences

THE UNIVERSITY OF TEXAS AT EL PASO

August 2024

Acknowledgements

I would like to extend my heartfelt gratitude to my advisor, Dr.Hernan Moreno of the Earth, Environmental and Resource Sciences Department at The University of Texas at El Paso, for his unwavering guidance, encouragement, enduring patience, constant support and expertise throughout this research endeavor. His insightful feedback with clear explanation, dedication and valuable time have been instrumental in shaping the thesis and scholarly development. He always encouraged me to give that immense driving energy that required to complete my job when I felt tired and got stuck. I wish all students the honor and opportunity to experience his ability to perform at that job.

I also indebted to the other members of my committee, Dr. Hugo Gutierrez of the Earth, Environmental and Resource Sciences and Dr. Marguerite Mauritz of the Biological Sciences, both at The University of Texas at El Paso. Their generous feedback, constructive criticism and scholarly contributions were invaluable to the completion of this work.

As a special note, Dr. Marguerite was extremely helpful in providing the additional guidance and resources I needed in order to complete my research activities, specially with sharing the Summer mircometerological data's from the US-Jo1: Jornada Experimental Range Bajada Site.

Additionally, I want to thank Department of Environmental Science and Engineering for providing the necessary resources, facilities and financial support to pursue my higher studies. Special thanks to department chair Dr. Craig Tweedie and Ms. Lina Hamdan for this valuable suggestions in my academic step. I am thankful to all the and professors and office staff of Department of Earth, Environmental and Resource Sciences for their support in every academic step. I am also grateful to department chair Dr. James Kubicki to provide financial support that helped me to attend American Geophysical Union Annual Meeting.

I extend my appreciation to the GeoSenSE lab mates and Director Dr. Laura Alvarez for their intellectual exchange, and moral support. Their encouragement have been a source of inspiration and motivation during challenging phases. I want to specially thank Santiago Hoyos, Jorge Mayo, Jayanga Samarasinghe and Stephanie Marquez for their contributions on my research development.

My deepest gratitude goes to my wonderful family for their unconditional love, sacrifice and patience. Their endless support and belief in my abilities have been the key motivation of my academic pursuits. I am immensely grateful to my wife, Humayra Afrin for her enduring support through the challenges and triumphs of this journey. I am also extremely lucky to share my joyous time with my precious babies, Izhaan Rahman and Ibtihaj Rahman. I owe an immeasurable debt of graditude to my parents for installing in me a passion for learning, resilence in the challenging times and values of intergrity and hard work.

NOTE: This thesis was submitted to my Supervising Committee on the August 9, 2024.

Abstract

This study proposes a new method for computing transpiration across an eddy covariance footprint using field observations of plant sap flow, phytomorphology sampling, uncrewed aerial system (UAS) digital image processing, and eddy covariance micrometeorological measurements. The method is applied to the Jornada Experimental Range, New Mexico where we address three key questions: (1) How do daily summer transpiration rates of Mesquite *(Prosopis glandulosa)* and Creosote *(Larrea tridentate)* individuals of different ages compare? (2) How can the contributions of plants of varying sizes and ages be integrated for terrain-wide transpiration estimates? (3) What is the contribution of transpiration to total evapotranspiration within the eddy covariance footprint? Data collected from June to October 2022, during the North American Monsoon season, include hourly evapotranspiration and precipitation rates from the Ameriflux eddy covariance system (US Jo-1 Bajada site) and sap flux rates from heat-balance sensors. We used plant biometric measurements and supervised classification of RGB imagery to upscale from the patch- to footprint-scale estimations. Our results show that Mesquite's average daily summer (JJAS) transpiration is about 2.9 mm/day, while Creosote's is 1.7 mm/day. A proportional relationship between the plant's horizontal projected area and the number of water flow conduits was extended to the eddy covariance footprint via UAS data. The summer transpiration to evapotranspiration ratio (T/ET) was 0.52, increasing to 0.83 following significant precipitation in September 2022. Further testing of this method is needed in different regions to validate its applicability. With appropriate adjustments, it could be relevant for other areas with similar ecological conditions.

Table of Contents

List of Tables

List of Figures

Chapter 1

Introduction & Background

Partitioning evapotranspiration (ET) is crucial for comprehensively understanding the water balance across diverse ecosystems, including those in arid conditions, complex terrain, or under intense anthropogenic influence [64]. By discerning the individual contributions of evaporation (E) from soil and wetted surfaces and transpiration (T) from vegetation, researchers can better parameterize land surface-atmosphere models and understand the relationships between soil moisture, atmospheric demand, carbon fluxes, and stocks.

ET partitioning is particularly interesting in arid and semi-arid regions where water scarcity is a pressing issue and vegetation succession is undergoing [62]. While ET in dryland ecosystems has been successfully estimated using the Bowen Ratio [14, 36, 61] and open path Eddy Covariance techniques, the effects of changes in ecohydrological processes overtime on the partitioning of ET fluxes (e.g. Creosote bush expansion), remain poorly understood [41, 52]. However, it has been suggested that combining micro-meteorological (Bowen ratio or eddy covariance data), eco-physiological (sap-flow or isotopic measurements), hydrological (micro-lysimeters, tensiometers) and high-resolution remote sensing methods would allow for ET partitioning approximations [76, 78, 60].

Since most summer precipitation (P) events in dryland ecosystems are relatively few and modest in the northern Chihuahuan desert (i.e. southwestern USA; [51]), only the top few centimeters of the soil are typically saturated after rain showers, and the water is quickly consumed by soil evaporation (E) and shallow-root plant transpiration (T) due to the high atmospheric demand for water [6, 27, 59]. However, deeper soil moisture infiltrated

after stratiform winter and spring precipitation or intense, but rare, summer convective thundershowers is associated with higher contributions of T [37]. Previous research has shown that T/ET tends to be high after isolated, individual intense summer precipitation events [57, 69]. Another factor that controls the partitioning of ET is the depth of the soil horizon. The presence of indurated and spatially-continuous caliche ($CaCO_3$) layers limits deep ($> 1m$) water flow [15, 47] which favors shallow water accumulation (above and around the root-zone layer) and, therefore, vegetation water use for long periods [70]. In synthesis, despite other contributing factors, in arid and semi-arid regions, the frequency and strength of the precipitation pulses, the presence of a calcium carbonate horizon, and the spatial distribution and type of plant individuals affect the vertical distribution of soil moisture and consequently, the partitioning of ET [42, 35].

Inputs and outputs of water (e.g., P, E, T, and runoff R) to and from these ecosystems are intrinsically related to the soil-vegetation carbon budget. In the minutes following precipitation, there is a piston-like sudden release of volatile carbon from the soil [13, 18] that is then followed by a slower-pace increase in vegetation carbon capture via net plant productivity [27]. Unfortunately, data on the partitioning of ET and carbon exchange characteristics at an adequate temporal and regional scale are insufficient to understand these critical ecosystem transient states [60], and this is why information on how and when plants use soil moisture is still required [7, 52].

Only a few empirical studies have measured T/ET in semiarid shrublands over short periods due to the high cost associated with equipment maintenance and data retrieval [45] and their results present a wide range of estimations [54]. Long-term T/ET ratios in drylands are typically lower than 0.5, but in wetter climates, they can reach up to 0.7 [5]. However, daily rates by species individuals have rarely been estimated. [17] conducted a study in a semiarid northeastern Colorado shortgrass steppe from May 1999 to October 2001 using a basic isotopic mass balance technique. The sum of total T and E losses was comparable to the actual ET determined from a nearby Bowen ratio energy balance system. The amount of water lost by evaporation (E/ET) varied depending on when precipitation inputs were

received; it ranged from zero to roughly 40% during the growing season and up to 90% during the dormant season. [38] used commercially available gauges to determine the daily and seasonal water use of three-year-old Chardonnay plants in New Deal, Texas, to evaluate the applicability of the stem heat balancing method. According to their findings, the stem flow gauges' accuracy ranged from 5% to 10% of the daily transpiration amount as determined by gravimetric measurements. Inter-plant transpiration variability was significantly decreased when the area of its leaves normalized the total sap flow of each plant. [61] measured whole plant T using the heat balance, sap flow method, ET, and net ecosystem exchange (NEE) of CO_2 using the Bowen ratio approach. They discovered that E outnumbered T at the onset of the rainy season. E peaked and began to fall quickly after rain events once the rain started, while T often reached its peak hours (or sometimes days) following E and began to decrease subsequently, with T values proportional to the size of the precipitation pulse. An overarching observation is the lack of generalizing methods for extending individual plant T measurements over larger areas like those of eddy covariance footprints or ecosystem regions where the individual observations can be used as representative of the entire community dynamics.

The objectives of this study are to (1) find out how the dominant Mesquite *(Prosopis glandulosa)* and Creosote bush *(Larrea tridentata)* vegetation species, typical of the dryland southwestern United States use water under different summer weather conditions and to (2) propose and test an Unmanned Aerial System- (UAS) based method to scale up T/ET measurements over an eddy covariance footprint. This research uses a sap flux network of sensors installed in different-age Mesquite and Creosote individuals and measures their branch distribution, aiming to establish a biometric relation between T and branch density that serves as a basis to scale up an individual plant to their footprint-scale activity via UAS RGB imagery. Auxiliary variables from a nearby micro-meteorological station (i.e., ET and P) are also used. The T rate differences between Creosote and Mesquite might vary due to plant root depth, branch diameter, rainfall amounts, and water use efficiency (carbon fixed per water loss rates). With a better understanding of plant responses to precipitation and

soil moisture changes, it will be easier to explain the effects of global climate change and vegetation succession on semiarid ecosystems. The results from this research will help in land surface and hydrologic model calibration and validation efforts and are expected to serve as a standard method for ET partitioning at the eddy covariance footprint.

Chapter 2

Study Area

This research was conducted at the Jornada Experimental Range (JER) within the eddy tower footprint of the Ameriflux Bajada (US-Jo1) site in southern New Mexico (USA) in the northern range of the Chihuahuan desert (Figure 2.1). Roughly, the JER comprises 200,000 hectares of land within New Mexico's Dona Ana County. Within the study site (Figure 2.1a), vegetation is dominated by mixed shrublands, including honey Mesquite *(Prosopis Glandulosa)* and Creosote shrub *(Larrea Tridentata)* [66, 2]. Outside the study area, desert grasslands intermix with the shrubs [43]. The JER climate is characterized by a mean annual air temperature of 15 °C and an average annual precipitation of 233 mm (1991–2020) [4]. The lowest annual precipitation on record was 77.0 mm in 1953, and the highest was 507.2 mm in 1984. During the North American Monsoon season (JAS), the average diurnal minimum and maximum temperatures oscillate between 13°C and 36°C, with more than 50% of total annual precipitation occurring during these months. Details about the eddy footprint area (Figure 1a), such as mean elevation, soil textural types, terrain, and vegetation characteristics, are presented in Table 3.1.

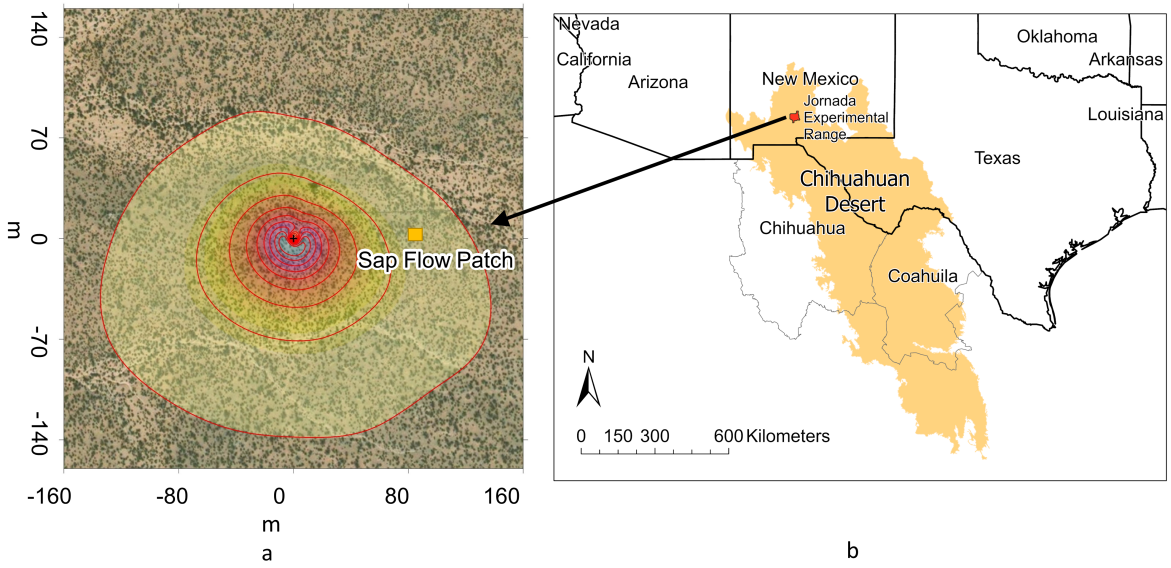

Figure 2.1: (a) Ameriflux Bajada (US-Jo1) eddy covariance flux footprint computed from the climatological approximation by [34] on an RGB raster image from the growing season (summer) of 2022. The outermost red contour line of the source area represents the region that contributes to the ET flux 10% of the time. Successive inward contour lines represent increments of 10% to the ET total flux up to 90%. The image also includes the location of the eight sapflow sensors (yellow box). (b) Location of the Chihuahuan desert and Jornada Experimental Range (JER) within the southwestern U.S.

Chapter 3

Material & Methods

3.0.1 Micrometeorological Measurements

This study's data analysis period is from June 1^{st} to September 30^{th} of 2022. At US-Jo1, P, ET, and other micro-meteorological and energy fluxes are continuously measured with quality control assurance]Anthony. P is continuously measured with a Texas Electronics Campbell Scientific tipping bucket rain gauge (TE525-L15-PT) while latent heat flux (λE) with an open-path gas analyzer (LI-7500 LICOR) sensor. The ET rate is then retrieved by converting energy λE (W.m^{-2}) to equivalent water flux (mm.day^{-1}) by using the latent heat of vaporization and density of water at the prescribed temperatures. All micrometeorological data are aggregated in daily steps.

3.0.2 Plant Sapflux Measurements and Transpiration Values

Besides the micrometeorological measurements of the US-Jo1 tower, a sapflow network of eight sensors was installed in May 28^{th} of 2022 to develop this study. Previous studies have successfully used these types of sensors, including in arid and semi-arid regions [68, 65, 33]. Eight EXO sap flow (SGEX) devices manufactured by Dynamax, Inc. were installed within the US-Jo1 eddy footprint on four Mesquite and four Creosote bushes in a sub-area (approximately 10 m x 10 m size), 85 m east of the US-Jo1 eddy tower (see Figure 2.1 and Figure 3.1).

Sap sensor installations were performed on plant individuals of different ages, including young and mature, and aimed to represent the observed range of species within the whole

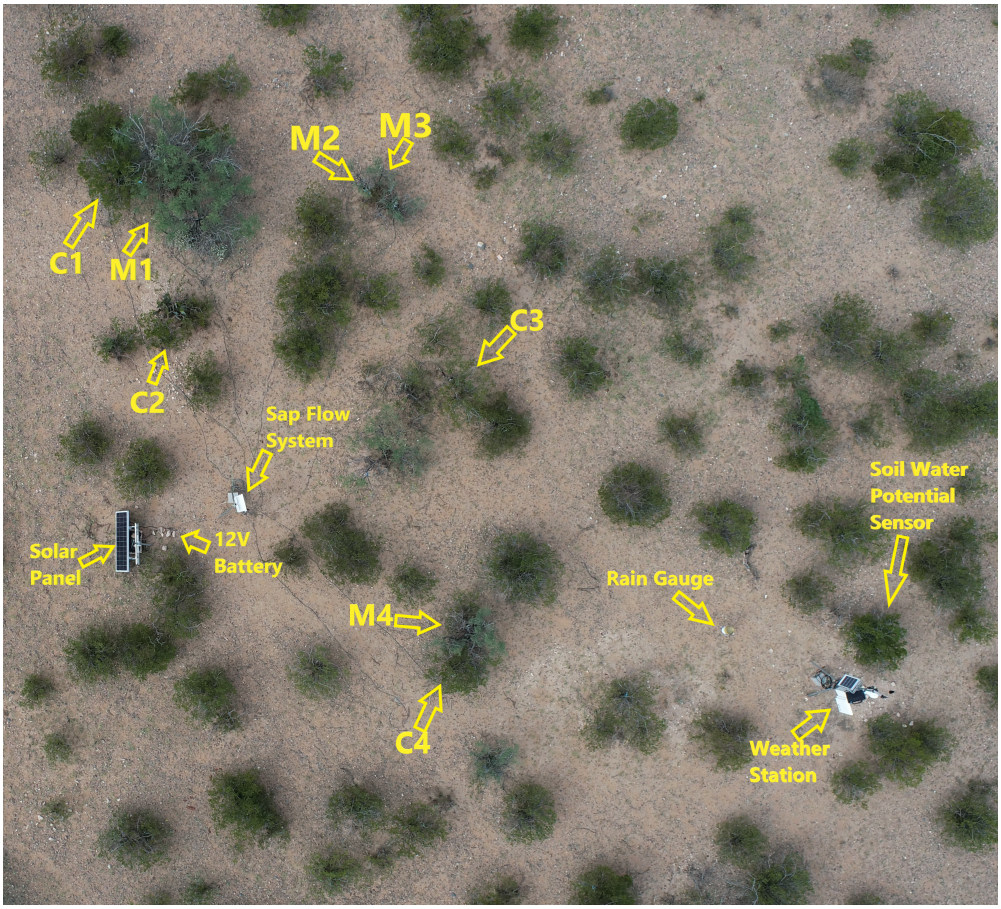

Figure 3.1: Sapflow patch area within the US-Jo1 eddy tower footprint. The aerial photogrammetry was accomplished using a small UAS 100 m above ground level (AGL). M1 through M4 are the four Mesquite, and C1 through C4 are the four Creosote individuals selected for sapflow monitoring. The picture also shows the location of solar panels, 12V deep cycle batteries, rain gauge, weather station, sapflow logger system, and soil moisture sensors. The centroid of this sapflow patch is located at approximate coordinates 32.5820° North and -106.6350° West and 1,188 m above sea level, about 85 m east of the US-Jo1 eddy tower.

Table 3.1: US-Jo1 eddy footprint areal characteristics including terrain, soil textural types, and vegetation [71]

Characteristic	**Values**
Elevation Range (m)	Min=1,376 m , Max=1,443 m
Areal Creosote Coverage	27%
Areal Mesquite Coverage	59%
Bare Soil Coverage	14%
Average Creosote Height	$< 1.5m$
Average Mesquite Height	$< 2m$
Soil Textural Types	Sandy Loam & Silt Loam
Caliche Layer Depth	Variable from 0 cm to 60 cm

eddy footprint (Figure 3.1). Figure 3.2 illustrates the typical sensor installation on a study branch (b) in a Mesquite individual at an arbitrary measurement height (H). Such a height, H that varied from 1 m to 1.25 m above ground, was determined individually for each tree according to the recommendations of the sap sensor manual to guarantee a minimum branch diameter to avoid malfunctioning. Installations required careful procedures as indicated by the system user manual. The selected stems were first cleared out with a pointed knife to prevent interference during the installation. Then, sandpaper was used to remove the stem's decaying bark to improve the sensors' contact with the cambium layer. Stems were then wiped with a paper towel and sprayed with canola oil to prevent sensors from adhering. The next stage was to wrap and stretch the double velcro to secure the heater stick's upper and lower thermocouple sections. Soft Gore-Tex material was used to prevent rainfall from penetrating the stem. The next layer of protection consisted of an insulating ring and reflective insulation material to prevent solar radiation from damaging stems [79]. At the top and bottom of the sap flow-installed stem, wire ties and tape were used to secure it. A data logger and a 12V, 100 Ah deep cycle battery were also installed to maintain the system continuously powered, along with a 75-85 Watt solar panel to provide energy to the system under sunlight. After installation, sensors were set to record heat fluxes at 1-min intervals (Δt) and then averaged and stored at 30-minute time steps on a Campbell Scientific CR1000X datalogger. Heat

fluxes measured by the system are then converted into water flux (F in g) using equation (1) as suggested by [56, 1].

$$F = \frac{P_{\text{in}} - Q_v - Q_r}{c_p \cdot \Delta T} \tag{1}$$

Where:

F = Total mass of sapflow transport (g) across the measuring branch b during time interval Δt.

P_{in} = Power input to the stem from the heater (W).

Q_v = The vertical or axial heat conduction through the stem (W).

Q_r = Rate of heat transfer through radiation (W).

c_p = Specific heat of water (J/g $\cdot^\circ$ C).

ΔT = Temperature increase of sap (°C).

During the measurement period, the M4 and C4 sapflow sensors malfunctioned due to extremely dry conditions, causing abnormally hot and prolonged periods without data. However, the other plant individuals recorded data correctly. Consequently, the malfunctioning sensors (M4 and C4) were excluded from the analysis. This type of sensor malfunctioning has been reported in previous studies during extremely dry conditions [8].

Sapflux sensors provide the total water flow across the branch diameter. This value has to be expressed per plant individual, assuming that the mass flux is approximately equal across all plant branches of the same individual for the same instant of time t, as suggested by [72]. Thus, equation (2) was derived to compute ${T_{ij}}^\bullet$ as the daily total T (g/d) of vegetation individual type i (e.g., Mesquite, M or Creosote C) and number j (e.g., 1, 2, 3, 4). Note that the next set of equations (2 through 8) provides a time series of values for each time step t at daily temporal resolution.

$$T_{ij}^{\bullet} = \frac{T_{ij}^{b}\ \overline{\phi}_{ij} N_{ij}}{\phi_{ij}^{b}} \tag{2}$$

Where,

T_{ij}^{b} = Measured daily transpiration (g/d) along branch b of plant ij.

$\overline{\phi}_{ij}$ = Average branch diameter (mm) at sensor height, H of plant ij (constant during the study).

N_{ij} = Number of branches (at sensor height, H of plant ij (constant during the study).

ϕ_{ij}^{b} = Diameter (mm) of branch b of plant ij where the sapflow sensor is installed (constant during the study).

A precision caliper was used to determine ϕ_{ij}^{b} and compute the distributions of all other ϕ_{ij} across the measurement height H. With $T_{ij}^{\bullet}$ values derived (in g/d), a subsequent relationship was derived to express this water mass flux as a water depth rate (T_{ij} in mm/d) dividing by the density of water, the typical Leaf Area Index (LAI_{ij}) of Mesquite and Creosote and the horizontally projected ground surface area (A_{ij}) that a tree occupies ([23] (equation 3).

$$T_{ij} = \frac{T_{ij}^{\bullet}}{\rho_w A_{ij} LAI_{ij}} \tag{3}$$

Where:

$T_{ij}^{\bullet}$ = Daily transpiration (g/d) of plant ij.

ρ_w = Density of water (0.001 g/mm; constant).

A_{ij} = Horizontal ground projection in mm^2 of plant ij (constant during the study).

LAI_{ij} = Leaf Area Index of plant ij (constant during the study but different for M and C).

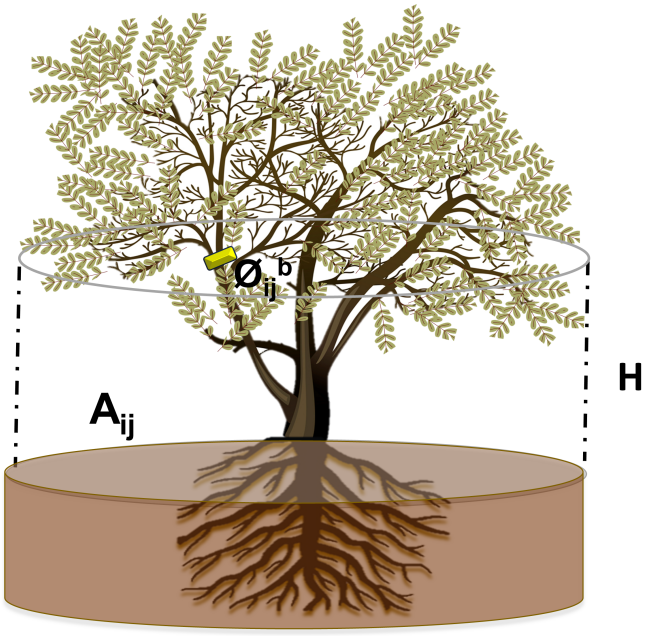

Figure 3.2: Schematic of a typical Mesquite bush sensor installation at branch "b" of diameter ϕ_{ij} (ϕ^b_{ij}) and other branches at the same height H. This H varies for each plant but roughly ranges from 1 m to 1.25 m above ground. N_{ij} is the total number of branches of different diameters ϕ at height H. i is the tree type (i.e., M or C), and j is the tree number (e.g., 1,2,3 and 4). Installations at all Mesquite and Creosote individuals mimic this description

A_{ij} was measured using low-altitude UAS imagery of each of the eight studied individuals. Since this study did not measure leaf area directly, values were obtained from results reported in the literature. According to several consulted studies [16, 58, 28] LAI of Chihuahuan desert Mesquite and Creosote individuals can vary depending on several factors, including the specific species, age, and environmental conditions. In general, the LAI for Mesquite trees ranges from about 1 to 3, and Creosote's between 0.5 and 2. Both species, particularly Mesquite, undergo leaf growth during the summer monsoon season due to higher temperatures and more water availability from the summer rains. Literature estimates provide Mesquite with LAI values ranging from 2 to 3 and Creosote between 1 to 1.5 ([23]. Since equation (3) needs a single value for both M and C, LAI_{Mj}=2.5 and LAI_{Cj}=1.25 were selected to

represent the typical conditions of summer in the Chihuahuan desert.

3.0.3 Individual Plant to Footprint Transpiration Rates

The areal extrapolation of the individual plant transpiration estimations (T_{ij}) via the sapflow network to the eddy tower footprint (T_{uv}), where u is either Mesquite or Creosote and v is the tree number within the footprint, was conducted by understanding: (A) the inter-plant variability of the term T^b_{ij}/ϕ^b_{ij} across the days, (B) the density function of ϕ_{ij} at each sensor level H for each of the eight sampled plants that allow to come up with a reasonable estimate of $\overline{\phi}_{ij}$, (C) The plant's horizontal projected areas A_{uv} that can be estimated via UAS remote sensing, and (D) A biometric relation between N_{uv} and A_{uv}.

(A) and (B) were determined when resolving the terms of equations (2) and (3) via the sapflow measurements and biometric characteristics of the sapflow patch. To resolve (C) and (D), small UAS flying 120 m above the ground during the growing season resulted in 3 cm pixel resolution images of the US-Jo1 eddy covariance footprint. The images were then mosaicked and geo-rectified using Agisoft Metashape. The resulting single image was then classified using a supervised methodology in ArcGIS Pro to obtain two single classes: Mesquite and Creosote. This classified image also allowed the measurement of A_{uv} as an attribute of each tree individual reflecting their age and other biometric characteristics. Along with the UAS flights, ground manual sampling was conducted to find N_{uv} for 33 (16 M and 17 C) individuals within the 70% source contribution contour line shown in Figure 1 as representative of the footprint vegetation to find a relationship between N_{uv} and A_{uv} (measured via UAS imagery).

Equation (4) was then applied to each plant individual of the classified image within the 10% source contribution area of Figure 1 at a daily time step for the study period. The ratio T^b_{uv}/ϕ^b_{uv} was taken as the mean T flux value per unit branch for all measured Mesquite or Creosote individuals within the sapflow network patch for each time step t (i.e., mean$[T^b_{ij}/\phi^b_{ij}]$). So this mean$[T^b_{ij}/\phi^b_{ij}]$ corresponds to two time series computed from the three independent measurements for Mesquite or Creosote species for each daily time step t

using equation (3).

$$T_{uv} = \frac{T^b_{uv}\ \overline{\phi}_{uv} N_{uv}}{\phi^b_{uv} \rho_w A_{uv} LAI_{uv}} \tag{4}$$

Where:

T_{uv} = Daily transpiration (g/d) of plant uv.

$\overline{\phi}_{uv}$ = Average branch diameter (mm) at sensor height, H of plant uv (constant during the study).

u = Tree type where 1 is M and 2 is C.

v = Tree number.

T^b_{uv}/ϕ^b_{uv} = Mean $\left[\frac{T^b_{ij}}{\phi^b_{ij}}\right]$ for M (u=i=1) or C (u=i=2).

N_{uv} = Number of branches at height H for individual uv(constant during the study).

ρ_w = Density of water (0.001 g/mm^3; constant.)

A_{uv} = Horizontal projection of ground covered area of plant uv in mm^2 (constant during study).

LAI_{uv} = Leaf Area Index of plant uv (constant for M and C during study).

With all T_{uv} estimations, an arithmetic average is computed following equation (5) to find out the total transpiration (T in mm/d) within the eddy footprint.

$$T = \frac{1}{n} \sum_{u=1}^{2} \sum_{v=1}^{n_M, n_C} T_{uv} \tag{5}$$

Where,

T = Total daily transpiration (mm/d) within footprint.

n = Total number of trees of all species within footprint.

u = Tree type. u=1 is M and u=2 is C.

v = Tree number.

n_M = Total number of M individuals within footprint.

n_C = Total number of C individuals within footprint.

Finally, equations 6 and 7 are used to understand the contribution of mesquite (M) or creosote (C) individually to the total daily T.

$$\overline{T_M} = \frac{1}{n_M} \sum_{u=1}^{n_M} T_{Mv} \tag{6}$$

$$\overline{T_C} = \frac{1}{n_C} \sum_{v=1}^{n_C} T_{Cv} \tag{7}$$

Where,

$\overline{T_M}$ = Daily T rate contribution for M over footprint.

$\overline{T_C}$ = Daily T rate contribution for C over footprint.

n_M = Total number of M individuals within footprint.

n_C = Total number of C individuals within footprint.

u = Tree type. u=1 is M and u=2 is C.

v = Tree number.

T_{Mv} = Transpiration rate of M individual v.

T_{Cv} = Transpiration rate of C individual v.

Chapter 4

Results

4.0.1 Biometric Measurements of Sapflow Patch Plants

Figure 4.1 (a and b) shows the fitted frequency distributions of plant branch diameters (ϕ_{ij}) at measurement height H for the 4 Mesquite (M) and 4 Creosote (C) individuals with sapflow sensors. The mean values ($\overline{\phi}_{ij}$) of these diameters are provided in Table 2. The data indicate that Mesquite individuals have branch diameters ranging from 6.8 mm to 18.3 mm, while Creosote individuals range from 5.1 mm to 12.3 mm. Among the Mesquite plants, M3 has the thinnest branches, whereas M1, M2, and M4 have thicker branches with narrower distribution spreads compared to M3. On the other hand, C individuals present slightly smaller mean diameter values (compared to all M), but their distributions appear more similar in terms of data dispersion around the mean.

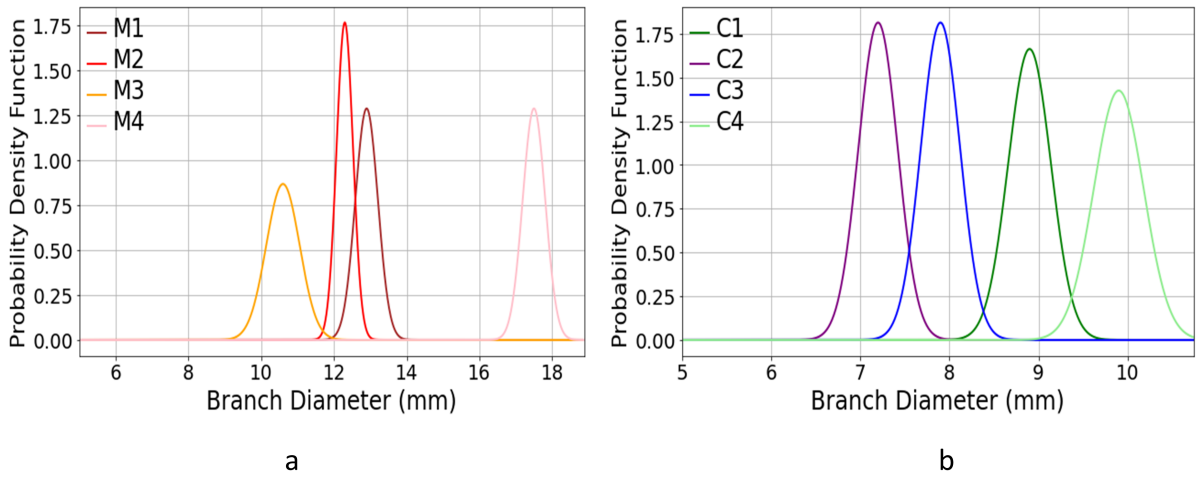

Figure 4.1: Probability density functions of the branch diameters, ϕ_{ij}, at the sensor measurement height (H) for the (a) four Mesquite and (b) four Creosote observed individuals

Table 4.1 presents the values of plant biometric features related to equations (2) and (3) for the sap flow-installed M and C plant branches. The branch diameter ranges with sensor installation (ϕ_{ij}^{b}) are 14.6 mm to 18.2 mm for M and 9.2 to 11.4 mm for C. These values are slightly larger than the average branch diameter values $\overline{\phi}_{ij}$ (Table 4.1, column 3) at height H (Figure 3.2) as suggested by the sensor manual to avoid overheating.

The ground projected areas A_{ij} (Table 4.1) appear similar across M and C individuals and perhaps related to age [46, 75] with values ranging from 0.62 m^2 to 2.8 m^2 for M and 1.16 m^2 to 2.0 m^2 for C. The largest areas are occupied by M1 (2.8 m^2), M4 (2.15 m^2), C1 (2.0 m^2) and C3 (1.92 m^2). Finally, the number of branches at height H (N_{ij}) illustrates values ranging from 14 to 20 for M and 20 to 28 for C. Therefore, although C individuals tend to have a smaller diameter, the number of branches tends to be higher on average at measurement height H compared to M individuals.

Table 4.1: Plant biometric features for the sap flow-installed sensors at ij plants. M means Mesquite, and C means Creosote (see Figure 3.1 for further spatial details).

Plant	ϕ^b_{ij} (mm)	$\overline{\phi}_{ij}$ (mm)	A_{ij} (m^2)	N_{ij}
M1	16.2	12.9	2.8	20
M2	14.6	12.3	0.94	16
M3	17.2	10.6	0.62	14
M4	18.2	17.5	2.15	17
C1	9.5	8.9	2	28
C2	9.2	7.8	1.16	25
C3	10.3	7.9	1.92	22
C4	11.4	9.9	1.27	20

4.0.2 Transpiration Rate Per Unit Branch Diameter

Figure 4.2 (a and b) illustrates a time series with precipitation (P; mm/d) and the ratio T^b_{ij}/ϕ^b_{ij} (g/mm.d; see equation 2) for each of the six observed trees (recall that M4 and C4 sensors suffered malfunctioning). Overall, T^b_{ij}/ϕ^b_{ij} responds to precipitation inputs in the subsequent days after the water inputs (note the sustained increase after the early September Monsoonal events in Figures 4.2 (a and b)). Figure 4.2(a) indicates that the three M individuals present similar T^b_{ij}/ϕ^b_{ij} with M1 and M3 more alike. Throughout the entire summer season, M2 displayed lower T^b_{ij}/ϕ^b_{ij} values in comparison to M1 and M3, except by some days when peaks were observed in M2, possibly due to temporary sensor malfunctioning or perhaps root-zone plant water access in the absence of significant recorded precipitation. Similarly, C individuals (Figure 4.2(b)) present consistent (but lower than M) T^b_{ij}/ϕ^b_{ij} values across the summer with increases after the September Monsoonal events. Overall, C2 and C1 present higher values than C3 over the measurement period.

4.0.3 Transpiration Rate Per Ground Covered Leaf Area

Figures 4.3 (a and b) show the behavior of plant transpiration T_{ij} (mm/d) for the sap flow-observed M (Figure 4.3(a)) and C (Figure 4.3(b)) individuals. The time series were

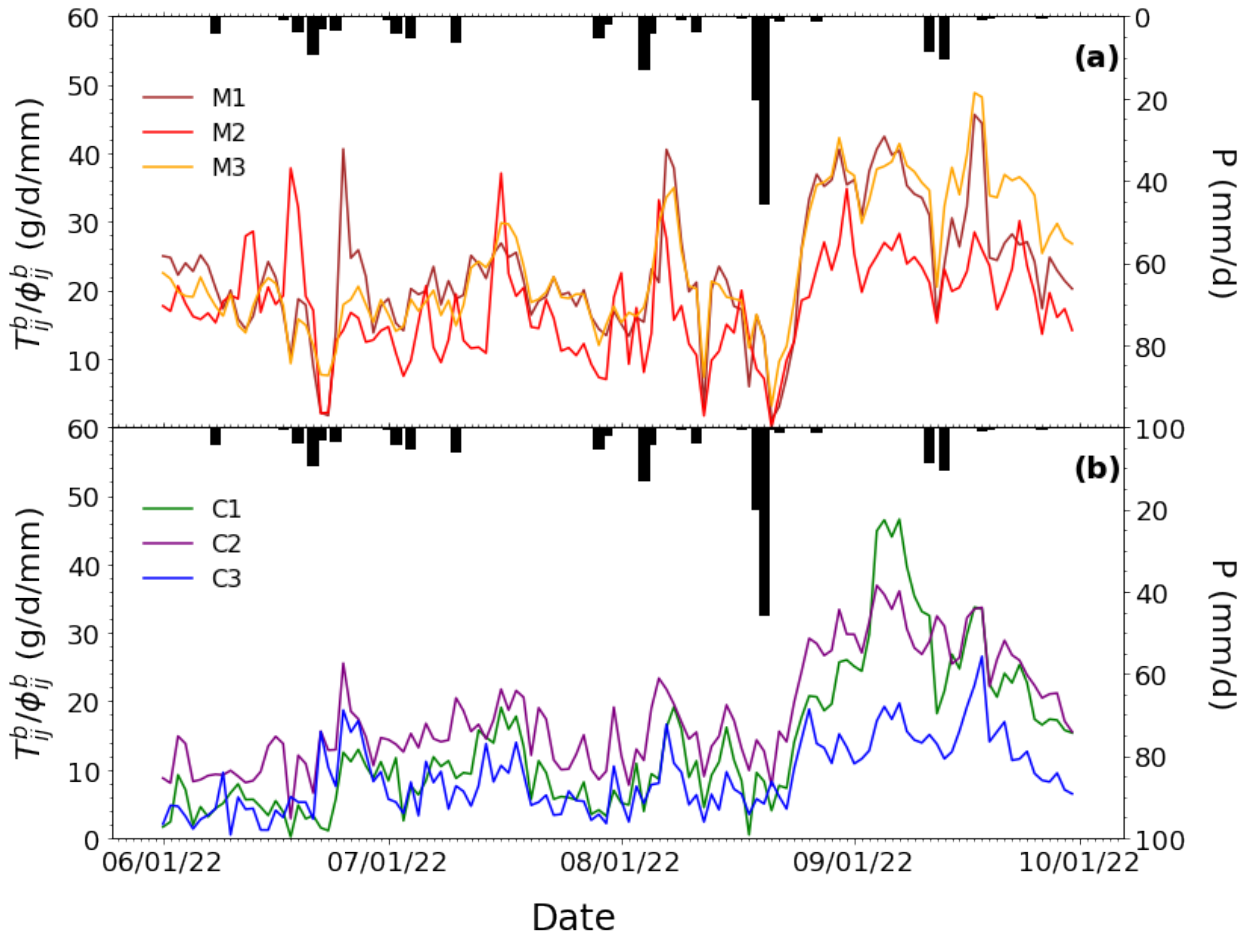

Figure 4.2: Daily time series of T_{ij}^b/ϕ_{ij}^b (g/mm.d) and P (mm/d) values on the sapflow-observed M and C tree branches during study period.

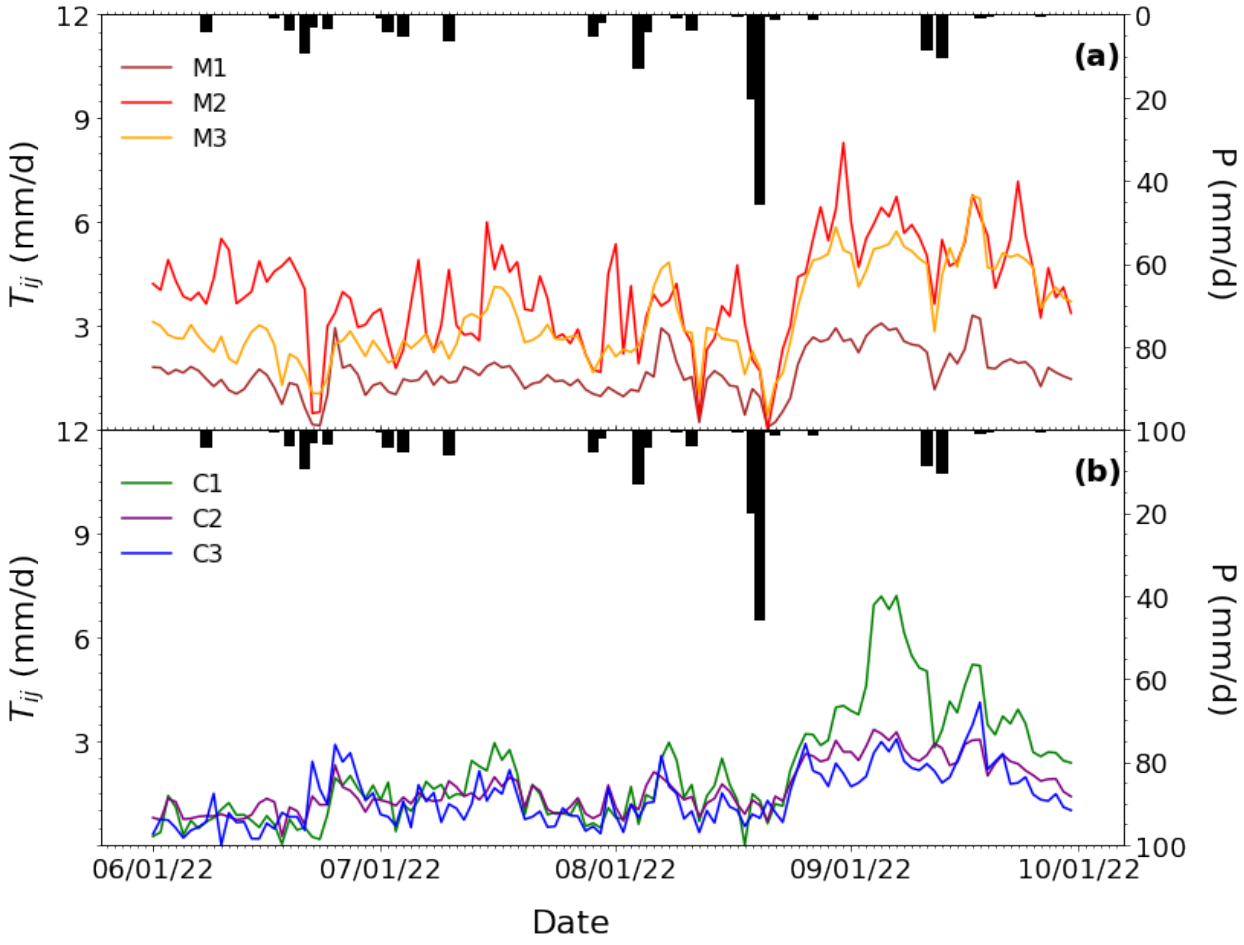

Figure 4.3: Daily time series of T_{ij} (mm/d) and precipitation (mm/d) for the sapflow-observed M and C trees during the study period

obtained after applying equation (3) with the values from Figure 4.2 and Table 4.1. Overall, the average daily T rates for the different individuals during the four months (JJAS) of 2022 are $\overline{T_{M1}}$=1.6 mm/d, $\overline{T_{M2}}$=4.0 mm/d, $\overline{T_{M3}}$=3.2 mm/d, $\overline{T_{C1}}$=2.1 mm/d, $\overline{T_{C2}}$=1.6 mm/d and $\overline{T_{C3}}$=1.4 mm/d. Average transpiration values for the 3 M ($\overline{T_{Mj}}$=2.9 mm/d) plants appear to be 1.7 times higher (on average) than those of C plants ($\overline{T_{Cj}}$=1.7 mm/d). This ratio appears to be mostly equal during the June to August period (drier conditions) when $\overline{T_{Mj}}$=2.4 mm/d while $\overline{T_{Cj}}$= 1.3 mm/d ($\overline{T_{Mj}}/\overline{T_{Cj}}$=1.8). On the other hand, when the strongest monsoon precipitation events appear in September, $\overline{T_{M2}}$=5.3 mm/d, $\overline{T_{M3}}$=4.8 mm/d while $\overline{T_{M1}}$=2.2 mm/d. For Creosote, the September storm showers resulted in a more significant increase in transpiration to $\overline{T_{C2}}$=2.5 mm/d $\overline{T_{C3}}$=2.2 mm/d and $\overline{T_{C1}}$= 4.3 mm/d. Across the month of September (rainier period) $\overline{T_{Mj}}/\overline{T_{Cj}}$=1.4 mm/d, which means that overall after precipitation occurs, Creosote bush increases their transpiration rates more significantly than Mesquite. C1, which has the highest number of branches across the C individuals (N_{C1}=28), appears to have the most significant T values across the C individuals during the drier and storm periods, sometimes approaching the M1 transpiration rates. The T_{M1} rates are the lowest of the 3 M individuals, perhaps due to the tree's low branch density per unit ground surface area.

4.0.4 Footprint-Scale Transpiration Rates

The areal estimation of total footprint transpiration used the UAS-derived RGB image shown in Figure 4.4 and the entire eddy covariance flux footprint (up to the 10% contribution area) illustrated by the contour lines of Figure 4.4. The number of M and C individuals within the footprint is 425 and 360, respectively. From the total footprint area, M and C cover 57% and 22%, respectively. Therefore, bare soil accounts for 21% of the surface footprint source area. These values are close to the ones reported in Table 3.1. To resolve equation (4) for the eddy footprint, N_{uv} was estimated by finding a relationship with A_{uv} (from Figure 4.4) within the 70% source area contour via the manual branch counting of 17 M and 17 C randomly-selected individuals at the same height H above the ground (H≈1 m). Figure 4.5

illustrates a proportional pattern between N_{uv} and A_{uv} that was approximated by near-linear relationships with a coefficient of determinations (R^2) above 0.85. Overall, Creosote plants show smaller covered areas ($0.5\ m^2 \leq A_{Cv} \leq 1.3\ m^2$) than Mesquite ($1.2\ m^2 \leq A_{Mv} \leq 3\ m^2$) while the number of branches is slightly higher for C ($18 \leq N_{Cv} \leq 27$) than M ($15 \leq N_{Cv} \leq 24$). Furthermore, the slope of the relationship between these two variables (N_{uv} vs A_{uv}) is higher for Creosote individuals.

Given the relative homogeneity of stem diameters across individuals of the same species, as shown by Table 4.1 and Figure 4.2, it was decided that $\overline{\phi}_{uv}$ should be taken as the mean value per species. So, for Mesquite, $\overline{\phi}_{Mv} = 13.6$ mm, while for Creosote $\overline{\phi}_{Cv} = 8.6$ mm. Concerning the T^b_{ij}/ϕ^b_{ij} to be applied to each of the uv trees, the results shown in Figure 5 support the selection of an average rate for all trees of the same species per time step t, as described in section 2.4. Based on the inputs mentioned above, T_{uv} was computed for every tree within the 10% contour of Figure 4.4 (i.e., the largest possible source footprint area), and after applying equations (4) and (5), results are shown in Figure 4.6.

Besides the time series of daily T (mm/d) values, Figure 4.6 also illustrates total daily P (mm/d) and the eddy-covariance measured ET (mm/d) values with commonly accepted error envelopes of 15% above and below the measurements [48, 12]. The total P during the JJAS summer period of 2022 was 168.1 mm, while the total ET was 140.2 mm and T= 73.4 mm. Therefore, for this period, ET/P= 0.83, T/ET=0.52, and E/ET= 0.48. Figure 9 also illustrates T values with an error envelope given by the uncertainty in T_{ij} computed as the mean absolute error of the variability introduced from Figure 4.3 (intra-individual variability) and the range of summer typical LAI values ($2 \leq LAI_{Mj} \leq 3$ and $1 \leq LAI_{Cj} \leq 1.5$; [23]).

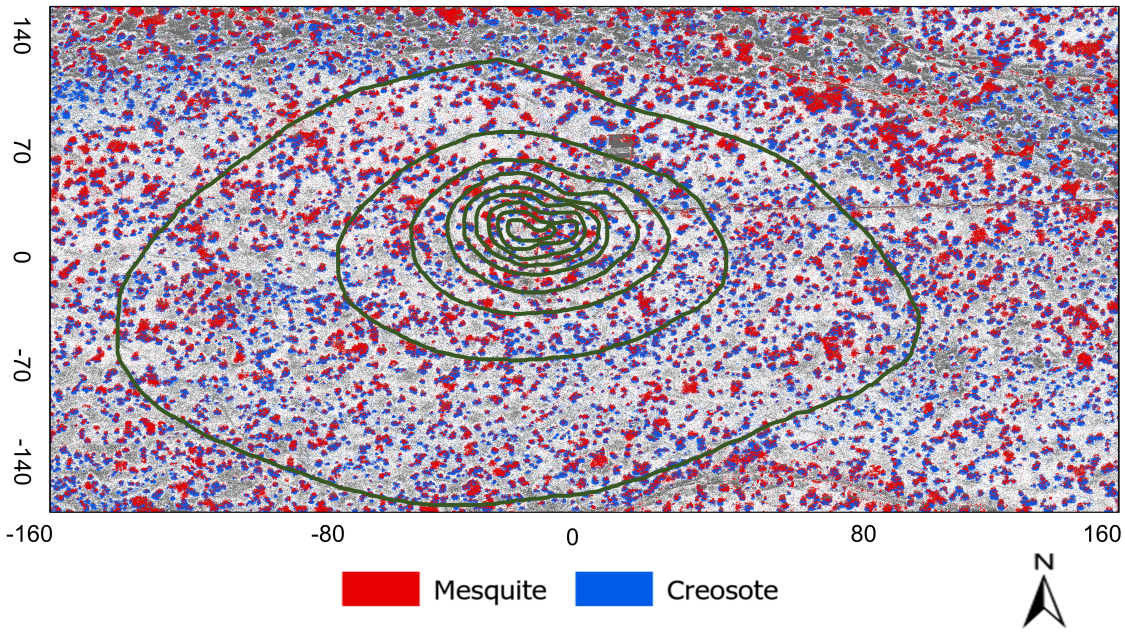

Figure 4.4: Supervised classification of UAS-obtained RGB image at 3 cm pixel resolution within the eddy footprint area of the US-Jo1 eddy covariance tower. The two main vegetation classes shown are Mesquite (red color) and Creosote (blue color). The outermost green contour represents the 10% (percent of the time) vapor flux source area, while subsequent inner contours represent increments of 10% in temporal contribution to total eddy-measured ET.

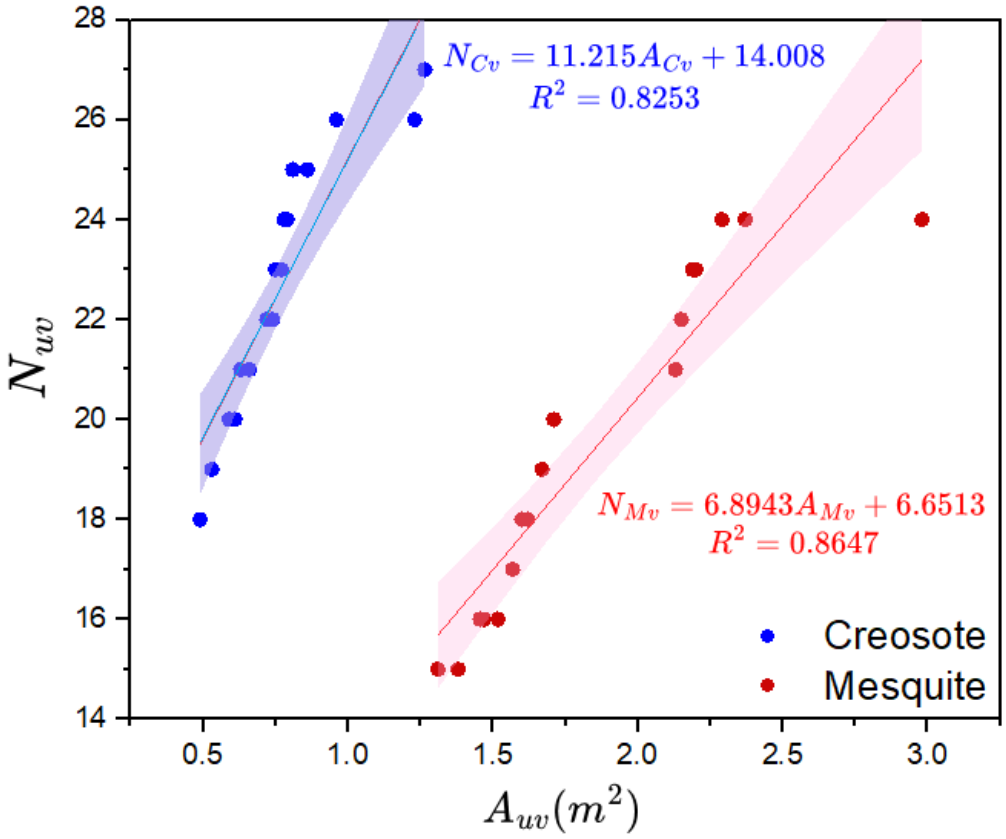

Figure 4.5: N_{uv} as a function of A_{uv} for 17 M and 17 C randomly selected individuals within the 70% ET contribution region. Linear regression equations are suggested with 20% uncertainty envelopes.

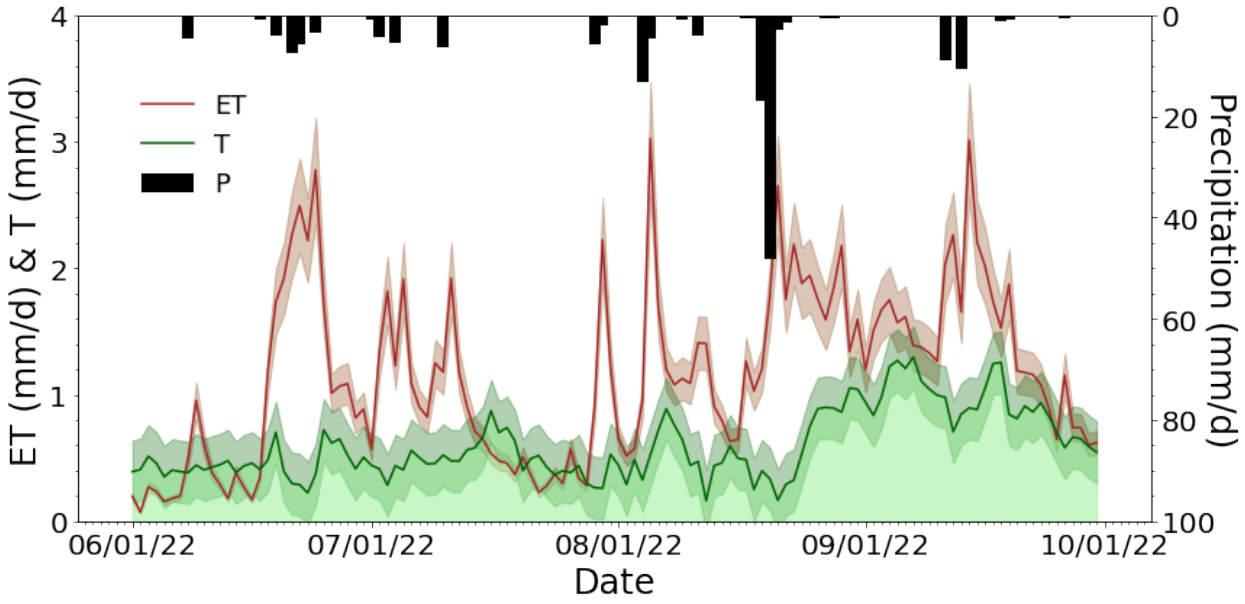

Figure 4.6: Mean daily precipitation P (mm/d), footprint evapotranspiration ET (mm/d) from the Ameriflux US_Jo1 eddy covariance system and transpiration T (mm/d) as computed from equations (4) and (5). The red and green envelopes around the estimated values represent the expected uncertainty as described in section 3.4.

Figure 4.6 shows that transpiration (T) is almost always below evapotranspiration (ET) and its error envelopes. It can be observed that the immediate response of ET to precipitation (P) events primarily comes from evaporation (E), while T shows delayed responses due to vegetation's slower access to water in the root zone, which can take several hours to days after the main storm events. However, once vegetation accesses root-zone water, T accounts for a more significant portion of ET while E is already experiencing a recession. During June, July, and August, with relatively low precipitation inputs (P=73.6 mm), ET values average 1.04 mm/day, while T averages 0.50 mm/day (T/ET=0.47). After the more intense precipitation events in early September (P=94.5 mm for the entire month), the mean ET values rise to 1.43 mm/day, and T rises to 1.19 mm/day (T/ET=0.83) on average from September 1^{st} to September 30^{th}.

Chapter 5

Discussion

This paper introduces and develops a methodology for estimating transpiration values across an eddy covariance footprint through the use of an in-footprint sapflow observation patch, the measurement of essential plant biometric features (i.e., typical branch diameter distributions and number of branches), and a low-altitude footprint ortho-photo. The method is applied to a (mostly homogeneous) fetch region with dominant Mesquite and Creosote bush species in the Jornada Experimental Range of the Chihuahuan Desert in southern New Mexico, United States. The results are assessed in terms of the total measured ET and analyzed regarding the precipitation inputs and the contribution of each plant species to the total T. Despite striving to come up with a physically-sound and practical method that incorporates high-resolution UAS imagery to scale measurements up from a smaller vegetation sap flux patch to the eddy covariance footprint region, the method relies on several assumptions that might pose limitations for its further use in other regions, but that can definitely encourage further tests and subsequent studies:

1. The different plant ages and sizes of the observed sapflow patch are representative of the footprint's plant distribution. This premise was confirmed after ground inspection of a representative sample of plant individuals within the 70% footprint that comprised individuals of different ages and sizes. Such a sampling method allowed to determine the best location of the monitored sapflow patch (Figure 1 and Figure 2). 2. Total sapflow transport values per plant (g/d) are proportional to the diameter and number of branches across each plant individual of different ages. This assumption implies that all live branches at the same

measurement height (H) are transporting sap at similar rates [3, 30] per unit branch cross-sectional area so that if this rate is multiplied by the number of branches, a total mass of sap transport per plant will be obtained.

3. To convert from mass flux (g/d) to depth rate (mm/d in Equation 3) the method needs to divide by the ground covered area of the plant and its Leaf Area Index. This mathematical artifact significantly simplifies the process. Sap flow rate measures the volume of water moving through plant tissues, but to estimate the actual transpiration rate and the amount of water loss through plant leaves per unit area, the expression needs to account for the total area of the canopy and the density of leaves. By dividing the sap flow rate by the ground surface area, the equation adjusts for the spatial scale of measurement, and dividing by LAI adjusts for the leaf density, providing a more accurate estimate of transpiration per unit area. This approach ensures that the resulting transpiration rate reflects the true water loss through plant foliage, helping to understand better water use efficiency.

4. There is a relationship between the number of branches at the same (hypothetical) sapflow measurement height H and the plant's ground projected area that can be extended to most (if not all) plants within the eddy footprint. The number of branches at a given sap flow measurement height H often indicates a plant's horizontal canopy coverage, which directly influences its transpiration rate. More branches generally correlate with a larger canopy area and, consequently, a higher transpiration rate, assuming other factors are constant [21, 49, 77, 32, 44].

5. Time series of values representing plant transpiration per unit plant diameter per species type are indispensable for accurately accounting for species-specific differences in transpiration within the eddy covariance footprint because these time series data provide critical insights into how various plant species contribute differently to overall water vapor fluxes. Plants of different species exhibit distinct physiological and structural characteristics that influence their transpiration rates, such as variations in leaf area, stomatal density, and hydraulic efficiency [22, 11, 50, 20, 39]. Additionally, using not one but several sapflow sensors across individuals of the same species is fundamental to understanding the physiologic and structural

differences among individuals of the same species but of different ages (or sizes) that allow capturing intra-species variability in transpiration rates.

The results obtained by this method (primarily synthesized in Figure 9) illustrate that T values (including their uncertainty envelopes) appear mostly below the measured eddy-flux ET values across the summer period, which fulfills the condition that $T \leq ET$. Additionally, consistent with previous studies [29, 74], evaporation (E) dominates evapotranspiration (ET) (E/ET=53%, T/ET=47%) when precipitation is scarce. After the summer monsoon events, transpiration (T) becomes the dominant contributor (T/ET=83%, E/ET=17%). Overall, across the North American summer monsoon season of 2022, our experiments concluded that both T and E contributed similarly to the whole ET water flux (T/ET=52% and E/ET=48%). This finding agrees with [63, 19, 55, 73] that support that roughly half of the water loss due to evapotranspiration is from plant transpiration, with the other half primarily from soil evaporation.

Several studies have attempted to partition evapotranspiration (ET) within the eddy covariance (EC) footprint region, including integration with remote sensing and modeling [24], energy flux partitioning from latent heat flux and sensible heat flux, catchment water balance [26, 31] and sapflow transects in adjacent areas [9] or via the measurement of LAI, FPAR (photosynthetically-active radiation) and vegetation fractional cover (FVC) [53, 80]. The latest often employs remote sensing data and mathematical modeling to estimate fractional vegetation cover (FVC) and LAI, which are then used to differentiate between the components of ET. For example, algorithms combining remote sensing data with regression methods, such as the random forest regression method, have shown reliable results in estimating FVC, which can be crucial for accurate ET partitioning [40]. Within the model-based approaches that include remote sensing data, a typical approach is to split ET according to the vegetation (FVC) and bare soil (FBC) fractions that are then used to find T and E (see Equations 8 and 9)

$$T = ET \times FVC \tag{8}$$

$$E = ET \times FBC \quad \text{or} \quad E = ET - T \tag{9}$$

If equations 8 and 9 were used in this study, the values found for T and E for the entire measurement period would be T=140.2 mm*(0.57+0.22)=110.6 mm and E=140.2mm*0.21=29.4 mm. With these values, T/ET = 79% and E/ET = 21%, which results in T/ET much higher than estimated here. The T/ET = 79% can be thought of as the maximum potential T (T overestimation) without LAI or hydraulic water transport considerations per plant species.

Despite the presented limitations, to the best of our knowledge, the novelty of this work can be summarized as follows:

1. Several previous studies have conducted field measurements across transects [9], used understory plant species in temperate forests [53], or combined species-specific data to improve accuracy in estimating ET at larger scales [80]. However, our method is the first to measure transpiration across an eddy footprint region using both inter- (two species) and intra- (six individuals) species sapflow rate measurements. This approach accounts for variability in physiological, hydraulic, and atmosphere-soil-plant interactions. Additionally, it transforms water mass flux rates to water depth rates using evaporative areal equivalences. These equivalences are measured by the Leaf Area Index and the ground-covered area for each plant.

2. The use of UAS to scale up sapflow hydraulic measurements for estimating transpiration (T) within an eddy footprint area is novel. Previous efforts with UAS had only produced high-resolution ET mapping [25, 67], or estimated ET via thermal and visible bands [10]. Our approach uniquely leverages UAS technology to enhance the accuracy of T estimations within the eddy footprint.

Finally, the results of this research are relevant and foundational in the new era of generative artificial intelligence for several reasons. Firstly, accurate partitioning into its components—transpiration (T) and evaporation (E)—provides high-quality training data for machine learning models, enhancing their predictive accuracy. This detailed data helps us

understand the underlying biophysical processes, leading to better model generalization across different environments. Furthermore, it enables the development of more precise and scalable ET models, critical for managing water resources, optimizing agricultural practices, and assessing ecosystem health in the face of climate change. By leveraging artificial intelligence, these partitioned observations can be integrated with satellite and UAS data to produce high-resolution, real-time ET estimates, thereby improving decision-making and resource management.

Chapter 6

Summary

This thesis presents a novel method for estimating transpiration within an eddy covariance footprint. By integrating plant sap flow measurements, phytomorphology sampling, UAS digital image processing, and micrometeorological data, valuable insights are gained into water use dynamics in arid ecosystems. Here are the key conclusions from their findings:

1. The average daily summer transpiration rates for Mesquite (Prosopis glandulosa) and Creosote (Larrea tridentata) were approximately 2.9 mm/day and 1.7 mm/day, respectively. The study also found that the transpiration to evapotranspiration (T/ET) ratio was 0.52 during the summer, which increased to 0.83 following significant precipitation events in September 2022.

2. The impact of precipitation on evapotranspiration dynamics was notable. During periods of scarce precipitation, evaporation and transpiration rates were similar (E/ET=53%, T/ET=47%). However, following summer monsoon events, transpiration became the dominant contributor to evapotranspiration (T/ET=83%, E/ET=17%), indicating that vegetation accesses root-zone water more significantly post-precipitation.

These findings are crucial for understanding plant responses to precipitation and soil moisture changes, which are vital for explaining the effects of global climate change and vegetation succession in semi-arid ecosystems. The study's results are valuable for land surface and hydrologic model calibration and validation efforts, providing a standard method for ET partitioning at the eddy covariance footprint level.

Looking forward, the developed method can be applied to other regions with similar

ecological conditions, with appropriate adjustments. The integration of UAS data with artificial intelligence to produce high-resolution, real-time ET estimates holds promise for improving decision-making and resource management in the face of climate change.

Chapter 7

Acknowledgement

This study is supported by the National Oceanic and Atmospheric Administration – Cooperative Science Center for Earth System Sciences and Remote Sensing Technologies under the Cooperative Agreement Grant #: NA22SEC4810016. The statements, findings, conclusions, and recommendations are those of the author(s) and do not necessarily reflect the views of NOAA.

References

[1] J. M. Baker and C. H. M. Van Bavel. Measurement of mass flow of water in the stems of herbaceous plants. *Plant, Cell & Environment*, 10(9):777–782, 1987.

[2] G. Bergametti and D. A. Gillette. Aeolian sediment fluxes measured over various plant/soil complexes in the chihuahuan desert. *Journal of Geophysical Research: Earth Surface*, 115(F3), 2010.

[3] Z Carter Berry, Nathaniel Looker, Friso Holwerda, León Rodrigo Gómez Aguilar, Perla Ortiz Colin, Teresa González Martínez, and Heidi Asbjornsen. Why size matters: the interactive influences of tree diameter distribution and sap flow parameters on upscaled transpiration. *Tree Physiology*, 38(2):263–275, 10 2017.

[4] Dawn M. Browning, Jason W. Karl, David Morin, Andrew D. Richardson, and Craig E. Tweedie. Phenocams bridge the gap between field and satellite observations in an arid grassland ecosystem. *Remote Sensing*, 9(10), 2017.

[5] Jingyi Bu, Guojing Gan, Jiahao Chen, Yanxin Su, Mengjia Yuan, Yanchun Gao, Francisco Domingo, Mirco Migliavacca, Tarek S. El-Madany, Pierre Gentine, and Monica Garcia. Dryland evapotranspiration from remote sensing solar-induced chlorophyll fluorescence: constraining an optimal stomatal model within a two-source energy balance model, 2022.

[6] D. H. Carlson, T. L. Thurow, R. W. Knight, and R. K. Heitschmidt. Effect of Honey Mesquite on the Water Balance of Texas Rolling Plains Rangeland. *Journal of Range Management*, 43(6):491, 11 1990.

[7] M. L. Cavanaugh, S. A. Kurc, and R. L. Scott. Evapotranspiration partitioning in semi-

arid shrubland ecosystems: a two-site evaluation of soil moisture control on transpiration. *Ecohydrology*, 4(5):671–681, aug 4 2010.

[8] Michelle L. Cavanaugh, Shirley A. Kurc, and Russell L. Scott. Evapotranspiration partitioning in semiarid shrubland ecosystems: a two-site evaluation of soil moisture control on transpiration. *Ecohydrology*, 4(5):671–681, 2011.

[9] Michelle L. Cavanaugh, Shirley A. Kurc, and Russell L. Scott. Evapotranspiration partitioning in semiarid shrubland ecosystems: a two-site evaluation of soil moisture control on transpiration. *Ecohydrology*, 4(5):671–681, 2011.

[10] Matthias Bernhardt Claire Brenner, Matthias Zeeman and Karsten Schulz. Estimation of evapotranspiration of temperate grassland based on high-resolution thermal and visible range imagery from unmanned aerial systems. *International Journal of Remote Sensing*, 39(15-16):5141–5174, 2018.

[11] Todd E. Dawson and James R. Ehleringer. Streamside trees that do not use stream water. *Nature*, 350(6316):335–337, March 1991.

[12] Tanja Denager, Majken C. Looms, Torben O. Sonnenborg, and Karsten H. Jensen. Comparison of evapotranspiration estimates using the water balance and the eddy covariance methods. *Vadose Zone Journal*, 19(1):e20032, 2020.

[13] Qi Deng, Dafeng Hui, Guowei Chu, Xi Han, and Quanfa Zhang. Rain-induced changes in soil co2 flux and microbial community composition in a tropical forest of china. *Scientific Reports*, 7, 12 2017.

[14] W. A. Dugas, R. A. Hicks, and P. Wright. Effect of removal ofJuniperus asheion evapotranspiration and runoff in the Seco Creek Watershed. *Water Resources Research*, 34(6):1499–1506, 6 1998.

[15] Michael Duniway, Jeffrey Herrick, and Curtis Monger. Spatial and temporal variability

of plant-available water in calcium carbonate-cemented soils and consequences for arid ecosystem resilience. *Oecologia*, 163:215–26, 12 2009.

[16] James R. Ehleringer, John Roden, and Todd E. Dawson. *Assessing Ecosystem-Level Water Relations Through Stable Isotope Ratio Analyses*, pages 181–198. Springer New York, New York, NY, 2000.

[17] Dom Ferretti, Elise Pendall, J.A. Morgan, J.A. Nelson, Daniel Lecain, and A.R. Mosier. Partitioning evapotranspiration fluxes from a colorado grassland using stable isotopes: Seasonal variations and ecosystem implications of elevated atmospheric co2. *Plant and Soil*, 254, 07 2003.

[18] Carrie-Ellen Gabriel and Lisa Kellman. Investigating the role of moisture as an environmental constraint in the decomposition of shallow and deep mineral soil organic matter of a temperate coniferous soil. *Soil Biology and Biochemistry*, 68:373–384, 2014.

[19] Stephen P. Good, David Noone, Naoyuki Kurita, Marion Benetti, and Gabriel J. Bowen. D/h isotope ratios in the global hydrologic cycle. *Geophysical Research Letters*, 42(12):5042–5050, 2015.

[20] Christopher M. Gough, Christoph S. Vogel, Hans Peter Schmid, and Peter S. Curtis. Controls on Annual Forest Carbon Storage: Lessons from the Past and Predictions for the Future. *BioScience*, 58(7):609–622, 07 2008.

[21] Michael L. Goulden, Bruce C. Daube, Song-Miao Fan, Douglas J. Sutton, Ammar Bazzaz, J. William Munger, and Steven C. Wofsy. Physiological responses of a black spruce forest to weather. *Journal of Geophysical Research: Atmospheres*, 102(D24):28987–28996, 1997.

[22] A. Granier, P. Biron, and D. Lemoine. Water balance, transpiration and canopy conductance in two beech stands. *Agricultural and Forest Meteorology*, 100(4):291–308, 2000.

[23] Kris M Havstad, Laura F Huenneke, and William H Schlesinger. *Structure and Function of a Chihuahuan Desert Ecosystem: The Jornada Basin Long-Term Ecological Research Site*. Oxford University Press, 08 2006.

[24] Mathias Herbst, Paul Rosier, David McNeil, and Richard Harding. Seasonal variability of interception evaporation from the canopy of a mixed deciduous forest. *Agricultural and Forest Meteorology*, 148:1655–1667, 10 2008.

[25] Helene Hoffmann, Rasmus Jensen, A. Thomsen, Hector Nieto, Jesper Rasmussen, and Thomas Friborg. Crop water stress maps for an entire growing season from visible and thermal uav imagery. *Biogeosciences*, 13:6545–6563, 12 2016.

[26] E.R Humphreys, T.A Black, G.J Ethier, G.B Drewitt, D.L Spittlehouse, E.-M Jork, Z Nesic, and N.J Livingston. Annual and seasonal variability of sensible and latent heat fluxes above a coastal douglas-fir forest, british columbia, canada. *Agricultural and Forest Meteorology*, 115(1):109–125, 2003. A tribute to George W. Thurtell's contributions in micrometeorology.

[27] Travis E Huxman, Bradford P Wilcox, David D Breshears, Russell L Scott, Keirith A Snyder, Eric E Small, Kevin Hultine, William T Pockman, and Robert B Jackson. Ecohydrological implications of woody plant encroachment. *Ecology*, 86(2):308–319, 2005.

[28] Travis E. Huxman, Bradford P. Wilcox, David D. Breshears, Russell L. Scott, Keirith A. Snyder, Eric E. Small, Kevin Hultine, William T. Pockman, and Robert B. Jackson. Ecohydrological implications of woody plant encroachment. *Ecology*, 86(2):308–319, 2005.

[29] Srijita Jana, Balaji Rajagopalan, Michael A. Alexander, and Andrea J. Ray. Understanding the dominant sources and tracks of moisture for summer rainfall in the southwest united states. *Journal of Geophysical Research: Atmospheres*, 123(10):4850–4870, 2018.

[30] K. H. Jensen, K. Berg-Sørensen, H. Bruus, N. M. Holbrook, J. Liesche, A. Schulz, M. A. Zwieniecki, and T. Bohr. Sap flow and sugar transport in plants. *Rev. Mod. Phys.*, 88:035007, Sep 2016.

[31] Chandra Jha, Kiran Chand Thumaty, Suraj Reddy, Ajit Sonakia, and Vinay Dadhwal. Analysis of carbon dioxide, water vapour and energy over an indian teak mixed deciduous forest for winter and summer months using eddy covariance technique. *Journal of Earth System Science*, 122:1259–1268, 10 2013.

[32] Gabriel Katul, David Ellsworth, and Chun-Ta Lai. Modeling assimilation and intercellular co2 from measured conductance. *Plant Cell and Environment - PLANT CELL ENVIRON*, 23:1313–1328, 12 2000.

[33] J.F. Kjelgaard, C.O. Stockle, R.A. Black, and G.S. Campbell. Measuring sap flow with the heat balance approach using constant and variable heat inputs. *Agricultural and Forest Meteorology*, 85(3):239–250, 1997.

[34] Natascha Kljun, Pierluigi Calanca, Mathias Walter Rotach, and Hans Peter Schmid. A simple parameterisation for flux footprint predictions. *Boundary-Layer Meteorology*, 112:503–523, 2004.

[35] Rebecca A. Kraimer, H. Curtis Monger, and Robert L. Steiner. Mineralogical distinctions of carbonates in desert soils. *Soil Science Society of America Journal*, 69(6):1773–1781, 2005.

[36] S. A. Kurc and E. E. Small. Dynamics of evapotranspiration in semiarid grassland and shrubland ecosystems during the summer monsoon season, central New Mexico. *Water Resources Research*, 40(9), 9 2004.

[37] S. A. Kurc and E. E. Small. Soil moisture variations and ecosystem-scale fluxes of water and carbon in semiarid grassland and shrubland. *Water Resources Research*, 43(6), 6 2007.

[38] R. J. Lascano, R. L. Baumhardt, and W. N. Lipe. Measurement of water flow in young grapevines using the stem heat balance method. *American Journal of Enology and Viticulture*, 43(2):159–165, 1992.

[39] Beverly E. Law and Richard H. Waring. Combining remote sensing and climatic data to estimate net primary production across oregon. *Ecological Applications*, 4(4):717–728, 1994.

[40] Duanyang Liu, Kun Jia, Haiying Jiang, Mu Xia, Guofeng Tao, Bing Wang, Zhulin Chen, Bo Yuan, and Jie Li. Fractional vegetation cover estimation algorithm for fy-3b reflectance data based on random forest regression method. *Remote Sensing*, 13(11), 2021.

[41] M. E. Loik, D. D. Breshears, W. K. Lauenroth, and J. Belnap. A multi-scale perspective of water pulses in dryland ecosystems: climatology and ecohydrology of the western USA. *Oecologia*, 141(2):269–281, may 8 2004.

[42] W. H. Schlesinger Marion and P. J. Fonteyn. Spatial variability of caco3 solubility in a chihuahuan desert soil. *Arid Soil Research and Rehabilitation*, 4(3):181–191, 1990.

[43] M. P. McClaran. Desert grasslands and grasses. *Unknown Journal*, pages 1–30, 1995.

[44] JL Monteith. Evaporation and environment. *Symposia of the Society for Experimental Biology*, 19:205—234, 1965.

[45] M.S. Moran, R.L. Scott, T.O. Keefer, W.E. Emmerich, M. Hernandez, G.S. Nearing, G.B. Paige, M.H. Cosh, and P.E. O'Neill. Partitioning evapotranspiration in semiarid grassland and shrubland ecosystems using time series of soil surface temperature. *Agricultural and Forest Meteorology*, 149(1):59–72, 2009.

[46] Karl Niklas. Plant allometry: The scaling of form and process. *Bibliovault OAI Repository, the University of Chicago Press*, 01 1994.

[47] M.M. Nobles, L. Wilding, and Henry Lin. Flow pathways of bromide and brilliant blue fcf tracers in caliche soils. *Journal of Hydrology*, 393:114–122, 10 2010.

[48] K.A. Novick, R. Oren, P.C. Stoy, M.B.S. Siqueira, and G.G. Katul. Nocturnal evapotranspiration in eddy-covariance records from three co-located ecosystems in the southeastern u.s.: Implications for annual fluxes. *Agricultural and Forest Meteorology*, 149(9):1491–1504, 2009.

[49] R. Oren, J. S. Sperry, G. G. Katul, D. E. Pataki, B. E. Ewers, N. Phillips, and K. V. R. Schäfer. Survey and synthesis of intra- and interspecific variation in stomatal sensitivity to vapour pressure deficit. *Plant, Cell & Environment*, 22(12):1515–1526, 1999.

[50] Ram Oren, David S. Ellsworth, K. H. Johnsen, Nathaniel Phillips, Brian E. Ewers, Claudia A. Maier, Klaus V. R. Schäfer, Helen McCarthy, George Hendrey, Stephen G. McNulty, and Gabriel G. Katul. Soil fertility limits carbon sequestration by forest ecosystems in a co2-enriched atmosphere. *Nature*, 411(6836):469–472, May 2001.

[51] M. Petrie, S. Collins, D. Gutzler, and D. Moore. Regional trends and local variability in monsoon precipitation in the northern Chihuahuan Desert, USA. *Journal of Arid Environments*, 103:63–70, 4 2014.

[52] D. L. Potts, T. E. Huxman, J. M. Cable, N. B. English, D. D. Ignace, J. A. Eilts, M. J. Mason, J. F. Weltzin, and D. G. Williams. Antecedent moisture and seasonal precipitation influence the response of canopyscale carbon and water exchange to rainfall pulses in a semiarid grassland. *New Phytologist*, 170(4):849–860, apr 25 2006.

[53] Jiabin Pu, Kai Yan, Guohuan Zhou, Yongqiao Lei, Yingxin Zhu, Donghou Guo, Hanliang Li, Linlin Xu, Yuri Knyazikhin, and Ranga B. Myneni. Evaluation of the modis lai/fpar algorithm based on 3d-rtm simulations: A case study of grassland. *Remote Sensing*, 12(20), 2020.

[54] James F Reynolds, Paul R Kemp, and John D Tenhunen. Effects of long-term rainfall variability on evapotranspiration and soil water distribution in the chihuahuan desert: a modeling analysis. *Plant Ecology*, 150(1):145–159, 2000.

[55] Y. Ryu, D.D. Baldocchi, T.A. Black, M. Detto, B.E. Law, R. Leuning, A. Miyata, M. Reichstein, R. Vargas, C. Ammann, Jason Beringer, L.B. Flanagan, L. Gu, L.B. Hutley, J. Kim, H. Mccaughey, E.J. Moors, S. Rambal, and T. Vesala. On the temporal upscaling of evapotranspiration from instantaneous remote sensing measurements to 8-day mean daily-sums. *Agricultural and Forest Meteorology*, 152:212–222, 2012.

[56] Tetsuo Sakuratani. A heat balance method for measuring water flux in the stem of intact plants. *Journal of Agricultural Meteorology*, 37(1):9–17, 1981.

[57] W. H. Schlesinger and S. Jasechko. Transpiration in the global water cycle. *Agricultural and Forest Meteorology*, 189-190:115–117, 6 2014.

[58] Susan Schwinning, Osvaldo E. Sala, Michael E. Loik, and James R. Ehleringer. Thresholds, memory, and seasonality: Understanding pulse dynamics in arid/semi-arid ecosystems. *Oecologia*, 141(2):191–193, October 2004.

[59] R. L. Scott. Using watershed water balance to evaluate the accuracy of eddy covariance evaporation measurements for three semiarid ecosystems. *Agricultural and Forest Meteorology*, 150(2):219–225, feb 15 2010.

[60] R. L. Scott, T. E. Huxman, W. L. Cable, and W. E. Emmerich. Partitioning of evapotranspiration and its relation to carbon dioxide exchange in a Chihuahuan Desert shrubland. *Hydrological Processes*, 20(15):3227–3243, 2006.

[61] R. L. Scott, T. E. Huxman, D. G. Williams, and D. C. Goodrich. Ecohydrological impacts of woody-plant encroachment: seasonal patterns of water and carbon dioxide exchange within a semiarid riparian environment. *Global Change Biology*, 12(2):311–324, jan 6 2006.

[62] Russell Scott and Joel Biederman. Partitioning evapotranspiration using long-term carbon dioxide and water vapor fluxes: New approach to et partitioning. *Geophysical Research Letters*, 44, 06 2017.

[63] Russell L. Scott, Joel A. Biederman, Erik P. Hamerlynck, and Greg A. Barron-Gafford. The carbon balance pivot point of southwestern u.s. semiarid ecosystems: Insights from the 21st century drought. *Journal of Geophysical Research: Biogeosciences*, 120(12):2612–2624, December 2015.

[64] Russell L. Scott, John F. Knowles, Jacob A. Nelson, Pierre Gentine, Xi Li, Greg Barron-Gafford, Ross Bryant, and Joel A. Biederman. Water availability impacts on evapotranspiration partitioning. *Agricultural and Forest Meteorology*, 297:108251, 2021.

[65] R. S. Senock and J. M. Ham. Heat balance sap flow gauge for small diameter stems. *Plant, Cell & Environment*, 16(5):593–601, 1993.

[66] Alfonso Serna Pérez, Curtis Monger, Jeffrey Herrick, and Leigh Murray. Carbon dioxide emissions from exhumed petrocalcic horizons. *Soil Science Society of America Journal*, 70, 05 2006.

[67] Jake E. Simpson, Fenner Holman, Hector Nieto, Ingo Voelksch, Matthias Mauder, Janina Klatt, Peter Fiener, and Jed O. Kaplan. High spatial and temporal resolution energy flux mapping of different land covers using an off-the-shelf unmanned aerial system. *Remote Sensing*, 13(7), 2021.

[68] D.M. Smith and S.J. Allen. Measurement of sap flow in plant stems. *Journal of Experimental Botany*, 47(12):1833–1844, 12 1996.

[69] X. Sun, B. P. Wilcox, and C. B. Zou. Evapotranspiration partitioning in dryland ecosystems: A global meta-analysis of in situ studies. *Journal of Hydrology*, 576:123–136, 9 2019.

[70] D. Szutu and S. Papuga. Year-round transpiration dynamics linked with deep soil moisture in a warm desert shrubland. *Water Resources Research*, 55, 07 2019.

[71] Craig Tweedie. Ameriflux fluxnet-1f us-jo1 jornada experimental range bajada site. *Unknown Journal*, 1 2022.

[72] Maurits Vandegehuchte and Kathy Steppe. Sap-flux density measurement methods: Working principles and applicability. *Functional Plant Biology*, in press, 04 2013.

[73] Enrique Vivoni, Carleen Aragon, Len Malczynski, and Vincent Tidwell. Semiarid watershed response in central new mexico and its sensitivity to climate variability and change. *Hydrology and Earth System Sciences*, 13, 06 2009.

[74] Enrique Vivoni, Hernan Moreno, Giuseppe Mascaro, Julio Rodriguez, Christopher Watts, Jaime Garatuza-Payan, and Russell Scott. Observed relation between evapotranspiration and soil moisture in the north american monsoon region. *Geophys. Res. Lett.*, 35, 11 2008.

[75] Richard H. Waring and William H. Schlesinger. *Forest Ecosystems: Concepts and Management*. Academic Press Inc., Orlando, San Diego, 1985.

[76] D. Williams, W. Cable, K. Hultine, J. Hoedjes, E. Yepez, V. Simonneaux, S. Er-Raki, G. Boulet, H. de Bruin, A. Chehbouni, O. Hartogensis, and F. Timouk. Evapotranspiration components determined by stable isotope, sap flow and eddy covariance techniques. *Agricultural and Forest Meteorology*, 125(3-4):241–258, 10 2004.

[77] Kell Wilson and Dennis Baldocchi. Comparing independent estimates of carbon dioxide exchange over five years at a deciduous forest in the southern united states. *Journal of Geophysical Research*, 106:34167–34178, 12 2001.

[78] E. A. Yepez, T. E. Huxman, D. D. Ignace, N. B. English, J. F. Weltzin, A. E. Castellanos, and D. G. Williams. Dynamics of transpiration and evaporation following a moisture

pulse in semiarid grassland: A chamber-based isotope method for partitioning flux components. *Agricultural and Forest Meteorology*, 132(3-4):359–376, 10 2005.

[79] Guangyang Yue, Halin Zhao, Tong Hui Zhang, Xueyong Zhao, Li Niu, and Sam Drake. Evaluation of water use of caragana microphylla with the stem heat-balance method in horqin sandy land, inner mongolia, china. *Agricultural and Forest Meteorology*, 148:1668–1678, 10 2008.

[80] Xubin Zeng, Robert E. Dickinson, Alison Walker, Muhammad Shaikh, Ruth S. Defries, and Jiaguo Qi. Derivation and evaluation of global 1-km fractional vegetation cover data for land modeling. *Journal of Applied Meteorology*, 39:826–839, June 2000.

Curriculum Vita

I am Habibur Howlider, an MS candidate from the department of Earth, Environmental Science and Resource Sciences. I completed my Bachelor Degree in Agriculture from Sher-e-Bangla Agricultural University, Bangladesh. After completing my bachelor study, I pursued my master's degree in the department of Environmental Toxicology at Texas Southern University, Houston. My research work was focused on chemical and geospatial analysis of soil and sediment samples collected from the Bayou and parks to observe the metal toxicity. also worked there as a environmental GIS analyst for couple of months before getting admission to The University of Texas at El Paso. I started working under the supervision of Dr. Hernan Moreno in the Department of Earth, Environmental, and Resource Science. In UTEP I work on measuring the partitioning from the eddy flux footprint evapotranspiration using the field and UAS observations in desert ecosystems. My MS research work was submitted to the Journal of Hydrology. While Pursuing a master's degree, I worked as a Graduate Teaching Assistant in Introduction to GIS and Earth Science courses.

Contact Information: hrhowlider@miners.utep.edu